Fluid dynamics based modeling of the Falcon concentrator for ultrafine particle beneficiation

Jean-Sébastien Kroll-Rabotin[a,*], Florent Bourgeois[a], Éric Climent[b]

[a] *University of Toulouse, Laboratoire de Génie Chimique, France*
[b] *University of Toulouse, Institut de Mécanique des Fluides de Toulouse, France*

Abstract

Enhanced gravity separators are widely used in minerals beneficiation, as their superior gravity field enables them to separate particles within narrow classes of density and size. This study aims to shed light on the Falcon concentrator's ability to separate particles within size and density ranges lower than usual, say 5 to 60 μm and 1.2 to 3.0 s.g. respectively. As differential particle settling is expected to be the prevailing separation mechanism under such conditions, this study presents the workings of a predictive Falcon separation model that embeds phenomenological fluid and particle flow simulation inside the Falcon's flowing film. Adding to the novelty of modeling the Falcon concentrator using a fluid mechanics approach, one point of practical significance within this work is the derivation of the Falcon's partition function from fluid flow simulation results.

Key words: Gravity concentration, Computational fluid dynamics, Modelling, Particle size

Introduction

Enhanced gravity separators are often used in mineral processing operations. Their fast rotating bowl generates an artificially enhanced gravity field several hundred times greater than Earth's gravity. Compared with one unit gravity, this produces a drastically augmented sedimentation velocity differential, such that enhanced gravity separators can process large flowrates of fine and ultrafine particles with a high separation efficiency (Chatterjee, 1998). As a result, enhanced gravity separators have been successfully used for beneficiating fine tailings (Venkatraman et al., 2000; Bradley et al., 2000).

Using a Falcon C40, Honaker et al. (1994) did obtain an ecart-probable $E_P = 0.12$ at a cut-point density of 1.6 s.g. with 1 mm $\times$ 0.075 mm fine coal particles. Such a performance was in fact better than that achieved using froth flotation. The efficiency of the Falcon concentrator for separating fine and ultrafine slurries, even with low density particles, makes it a strong candidate for beneficiating dredged sediments whose top size is normally below 100 μm. This study focuses on dredged sediments from harbours, rivers and lakes. Their typical make-up consists of three phases that we seek to separate with the Falcon concentrator: a valuable clean 100 μm $\times$ 10 μm sandy fraction, a minus 10 μm sandy fraction where pollutants concentrate, and an organic fraction. The sandy and organic fractions have specific gravity 2.65 and 1.3 respectively. Although particle size has a strong effect on the separation efficiency of enhanced gravity separators in the size range of interest (cf. §1.4), the favourable washability of dredged sediments gives us hope that the valuable fraction can be separated from the other two fractions on the basis of density. Deveau (2006) was able to concentrate particles in the 10 μm size range with a Falcon for heavy tantalum particles (16.6 s.g.): he was able to obtain an enrichment ratio of 10 and a recovery in excess of 70%. In order to assess whether the Falcon concentrator can possibly beneficiate dredged sediments, it is important to review the mechanisms that drive the separation inside an operating Falcon bowl.

Published studies have identified two distinct particle separation mechanisms inside the Falcon concentrator (Laplante et al., 1994; Laplante and Nickoletopoulos, 1997; Honaker et al., 1996; Abela, 1997): differential particle settling within the thickness of the liquid film that flows on the surface of the rotating bowl, and parti-

*Corresponding author
Email addresses:
jeansebastien.krollrabotin@ensiacet.fr (Jean-Sébastien Kroll-Rabotin), florent.bourgeois@ensiacet.fr (Florent Bourgeois), climent@imft.fr (Éric Climent)

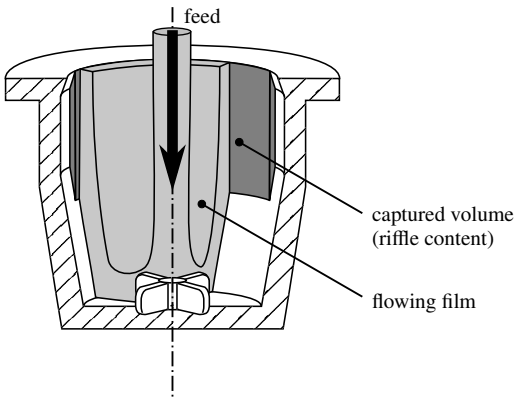

Figure 1: Schematics of the spinning Falcon smooth bowl

cle rearrangement inside the granular bed (Majumder et al., 2006) that forms inside the Falcon's retention zone. In the case of dense particles, as with fine gold for example, the second separation mechanism drives the separation, the heavier valuable particles being centrifuged against the bowl even before they reach the retention zone. However, with fine light particles, differential settling will condition the probability that a particle reaches the particle bed during its relatively short residence time inside the Falcon (Abela, 1997). Hence, the first separation mechanism is likely to become the dominant separation mechanism for dredged sediment beneficiation. Particle rearrangement inside the concentrate bed could in principle play a beneficial role in case light particles are entrained inside the particle bed, giving them an opportunity to be resuspended into the flowing film. This can be achieved by fluidizing the Falcon's retention zone (Abela, 1997; Laplante and Shu, 1993; Ancia et al., 1997). However, given the low inertia of dredged sediment particles, forced fluidization would most likely resuspend the whole particle bed. This explains why smooth non-fluidized bowls — as shown in figure 1 — are recommended for beneficiating fine and ultrafine particles (McAlister and Armstrong, 1998; Deveau, 2006).

Contrary to the Knelson separator (Honaker and Patil, 2002; Coulter and Subasinghe, 2005), a fluidisation-based enhanced gravity separator that is often compared to the Falcon (Laplante and Shu, 1993; Ancia et al., 1997), only a few mechanistic studies have been conducted with the Falcon. On the other hand, the Falcon has been the focus of several empirical studies (Honaker and Reed, 1995; Honaker and Wang, 1998; Honaker and Das, 2004; Holtham et al., 2005; Zhao et al., 2006). By measuring separation efficiency under controlled operating conditions, Laplante et al. (1994) and Laplante and Nickoletopoulos (1997) have derived a separation model for the Falcon concentrator. Through interpretation of their results, they identified and discussed separation mechanisms that most likely take place inside the Falcon; however, the model they derived in the end is utterly empirical and does not embed any physics of the separation. Honaker et al. (1994, 1996) undertook detailed work about the role of the particle bed on recovery; logically they concentrated their efforts on Falcon bowls that use fluidisation. Finally, Deveau (2006) investigated the relation between bed composition and the quality of the separation for fine particles. They showed that a layer of better quality concentrate builds on the surface of the bed, which agrees with our hypothesis that differential settling plays a key role for ultrafine particle separation. Indeed, should bed rearrangement occur with fine particles, the surface of the bed should contain the lighter and finer particles, those most susceptible to be resuspended. However, it turns out that the region of the bed with the highest quality, in terms of separation, is in fact the one where the sedimenting particles just enter the bed. Ultrafine particles having low inertia, it is expected that they cannot clear themselves a path towards the inside of the particle bed. This observation confirms the conclusion by Luttrell et al. (1995) that particle bed rearrangement is not suitable for the recovery of ultrafine particles with a Falcon concentrator.

The abovementioned mechanisms are radically different; yet they both influence particle separation to a degree that depends on the operating conditions and the washability of the suspension fed to the Falcon concentrator. It does not seem possible to delineate their respective contribution experimentally, i.e. by measuring the Falcon's product and reject streams under controlled experimental conditions. Therefore, in order to shed light on the effect and limitations of differential settling, which we believe is the driving mechanism for separating fine light particles, we have chosen to investigate particle transport inside the Falcon by computer simulation. The paper presents the building blocks of the physical model we use for simulating the transport of ultrafine particles in a smooth Falcon bowl with no fluidization. Simulation results on particle trajectory and scaling rules are also presented, from which the Falcon's partition curve can be derived. Eventually, experiments will be carried out using a L40 Falcon concentrator in order to test the validity of the hypotheses used in our model, such that numerical simulation can be used to predict the performance of Falcon concentrators for fine light particle separation.

1. Hydrodynamic modeling of the Falcon separator

1.1. Working hypotheses

Our numerical model is based on a number of hypotheses we believe are adapted to light ultrafine particles separation in a Falcon concentrator. The most important one is that particle separation is driven by differential sedimentation inside the flowing film. We therefore discard the possibility that particles be resuspended from the particle bed back into the flowing film. Under such an assumption, bed composition and granular flow within the bed are not needed, the particle bed acting as a particle sink. Once the trajectory of a particle enters the geometrical boundaries of the bed, which is set by the configuration of the bowl, and provided the bed is not already filled with particles, the particle in question enters the bed never to be seen again. Our problem is thus limited to the study of particle trajectories inside the rotating flowing film, from which we shall explore the separation capability of the Falcon concentrator for fine light particles (cf. figures 1 and 2).

Particle transport inside the film is controlled by the flow near the wall of the bowl. This flow could be perturbed by the presence of the particles beyond a critical solid volume fraction. Even without any such perturbation of the flow field, particle-particle collisions and particle entrainment through collective effects will become too high beyond a critical solid volume fraction. Such interactions will hinder the transport mechanisms that we seek to observe. Hence, we shall restrict our domain of investigation to dilute suspensions, such that particles have no effect on the flow field and particle-particle interactions can be neglected. From our experience with direct numerical simulation, such a hypothesis is strictly valid for solid concentrations below 5 vol.%. We believe that the configuration of the Falcon bowl will allow us to relax this constraint significantly. Given that our modelling approach permits evaluation of the perturbation induced by particle-particle interaction, our model will be eventually extended to concentrated suspensions.

A 4-blade impeller is mounted on the bottom of the Falcon bowl. This impeller ensures that the feed that hits the bottom of the bowl instantaneously rotates with the bowl. The artificially enhanced gravity induced by the rotation then drains the film upward along the angled wall of the bowl. The film thickness depends essentially on the feed flow rate and the rotational velocity. The thickness of the film is imposed by the impeller at the bottom of the bowl. It then varies along the wall length due to the angle of the bowl, which yields a continuous increase in both section and centrifugal force with

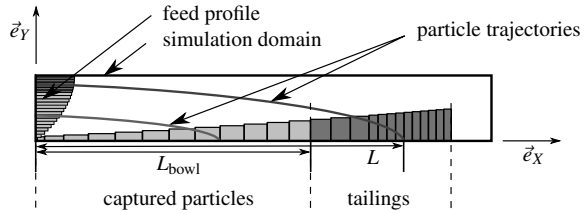

Figure 2: Numerical simulation: Lagrangian tracking of point particles

bowl length, and due to the no-slip viscous flow condition at the wall. Since both our visual observation and preliminary Volume of Fluid simulation (cf. §1.2) results indicate sub-millimetre film thickness, we have hypothesised that the variation of the film thickness can be neglected along the length of the L40 UF Falcon bowl that we use for our experimentations. Hence the simulations that are presented hereafter consider a constant film thickness. This hypothesis will be validated by numerical simulation (cf. §1.2).

Moreover, we assume that the impeller that gives the feed its initial rotational velocity mixes particles homogeneously as they enter the flowing film. In other words, we consider that particles are uniformly distributed in the thickness of the flowing film at the bottom of the bowl.

1.2. Numerical simulation

We aim at computing the particle trajectories. Therefore, based on a simple force balance (1) the particle acceleration (velocity and position) is related to the local fluid flow properties. We assume that the particulate phase is composed of non-interacting spheres (fixed radius r_p and density ρ_p). Also, we make the assumption of point particle while we neglect the velocity perturbation of the carrying fluid flow: the particle size is smaller than all the relevant flow scales.

$$\rho_p \mathcal{V}_p \frac{\mathrm{d}\vec{v}}{\mathrm{d}t} = \sum \vec{F} \tag{1}$$

The force balance accounts for different contributions. The main forces acting on the particles during their motion through the fluid film are the buoyancy force ($\vec{F}_B$) due to the density difference between the particles and the fluid, the pressure gradient effect ($\vec{F}_G$), the added mass force ($\vec{F}_M$) due to inertia of the fluid during an acceleration either of fluid or the particle and the drag force ($\vec{F}_D$) (Clift et al., 1978) accounting for the viscous

and pressure contributions:

$$\vec{F}_B = (\rho_p - \rho_f)\,\mathcal{V}_p\,\vec{g} \tag{2a}$$

$$\vec{F}_G = \rho_f \mathcal{V}_p \frac{\mathrm{D}\vec{u}}{\mathrm{D}t} \tag{2b}$$

$$\vec{F}_M = \rho_f \mathcal{V}_p C_M \left(\frac{\mathrm{D}\vec{u}}{\mathrm{D}t} - \frac{\mathrm{d}\vec{v}}{\mathrm{d}t}\right) \tag{2c}$$

$$\vec{F}_D = \frac{1}{2}\,\rho_f \mathcal{A}_p C_D \left|\vec{u} - \vec{v}\right| (\vec{u} - \vec{v}) \tag{2d}$$

The added mass coefficient (C_M) is set to $1/2$ as recommended by Magnaudet et al. (1995). The drag coefficient is calculated with the particulate Reynolds number (Clift et al., 1978) which asymptotically tends to the Stokes law when $Re_p \ll 1$:

$$C_D = \frac{24}{Re_p}\left(1. + 0.15 Re_p^{0.687}\right) \tag{3}$$

The forces (2b), (2c) and (2d) depend on the fluid velocity ($\vec{u}$) and its spatial gradient when the flow is steady. The force balance may be supplemented by other forces such as lift, history forces and wall corrections to the drag and added-mass effects. In the present paper we neglect those contributions. Rearranging the force balance the Lagrangian tracking of the particle is obtained by the numerical integration of equation (1).

$$\left(\rho_p + \rho_f C_M\right)\frac{\mathrm{d}\vec{v}}{\mathrm{d}t} = \rho_f\,(1 + C_M)\,\frac{\mathrm{D}\vec{u}}{\mathrm{D}t} + (\rho_p - \rho_f)\,\vec{g} - \frac{3}{8\,r_p}\rho_f C_D \left|\vec{v} - \vec{u}\right| (\vec{v} - \vec{u}) \tag{4}$$

The flow and the trajectories have a rotation symmetry therefore we only need the expression of the trajectory equations in a fixed azimuthal plan. Assuming that the slip between the particle and the fluid is negligible in the azimuthal direction ($v_\theta = u_\theta$), we can simplify the trajectory equation yielding:

$$\left(\rho_p + \rho_f C_M\right)\frac{\mathrm{d}\vec{v}_{2\mathrm{D}}}{\mathrm{d}t} = \rho_f\,(1 + C_M)\,\frac{\mathrm{D}\vec{u}_{2\mathrm{D}}}{\mathrm{D}t} + (\rho_p - \rho_f)\left(\frac{u_\theta^2}{r^2}\vec{r} + \vec{g}\right) - \frac{3}{8\,r_p}\rho_f C_D \left|\vec{v}_{2\mathrm{D}} - \vec{u}_{2\mathrm{D}}\right| (\vec{v}_{2\mathrm{D}} - \vec{u}_{2\mathrm{D}}) \tag{5}$$

The projection of the force balance in the azimuthal direction does not need to be solved. We assume that the slip velocity is very small because the projections of the buoyancy and centrifugal forces stand only in the plane of simulation containing the axis of rotation symmetry. However, solving only the two-dimensional projection of the particle transport equations does not prevent a full three-dimensional solution of the Navier-Stokes equations for the fluid velocity which controls the variation of the azimuthal velocity of the fluid across the film section.

All the fluid information is computed at the precise location of the particle centre. The fluid velocity field is predicted by a direct numerical solution of the Navier-Stokes equations (incompressible fluid) on a fixed mesh grid where typical grid cells are much larger than the particle width:

$$\nabla \cdot \vec{u} = 0 \tag{6a}$$

$$\frac{\partial \vec{u}}{\partial t} + (\vec{u} \cdot \nabla)\,\vec{u} = -\frac{1}{\rho_f}\nabla p + \nu_f \nabla^2 \vec{u} \tag{6b}$$

The fluid flow equations are solved in a conservative form using the finite volume method on a staggered grid. The velocity profile is imposed at the inlet (parabolic profile which verifies the no-slip boundary condition on the bowl wall and a zero shear stress on the air/water interface) and we assume that the thickness of fluid film is constant. The flow leaves the computational domain due to the selection of an output numerical condition.

Even with a small cone angle of the bowl (20°), the high rotation rate induces a significant Coriolis force $\omega u_r \sin(\beta/2)$ in the simulation plane. A balance between the driving force and the viscous effects in the wall region gives a rough estimate of the flow boundary layer in the film. The theoretical prediction of the film thickness evolution along the bowl wall could be an issue. This point has been addressed by preliminary studies by Bruin (1969), Makarytchev et al. (1997, 1998), Janse et al. (2000) and Langrish et al. (2003) who were interested in spinning cone columns. Also, this aspect of the process may be investigated by a numerical approach dedicated to the interface motion, for instance: the Volume of Fluid method (Dijk et al., 2001). We expect only weak variations of the film thickness, therefore we assume in the present paper that the film thickness, the fluid flow rate and the rotation rate of the bowl are fixed and may be varied independently around the operating condition we selected. We have made some simulations to test the sensitivity of the results to the film thickness imposed in the simulation. Above a certain film depth the velocity profile corresponds to a pure solid rotation where the streamwise velocity along the bowl wall is close to zero. Therefore, this region of the film does not contribute to the mass flow rate of the suspension and

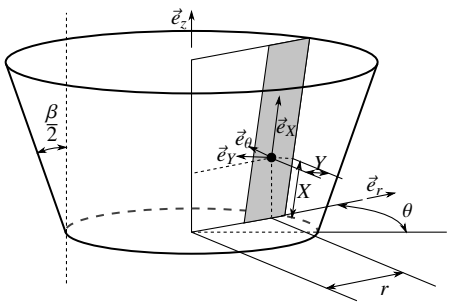

Figure 3: Coordinate systems

does not modify our results on the performance of the Falcon separator. The fluid flow boundary layer in the vicinity of the bowl wall is likely to be a good estimate of the film thickness.

1.3. Solid fraction trapped in the bowl

Based on our assumption that all particles that enter the retention zone of the Falcon remain fixed until the end of the separation cycle (cf. §1.1), the criterion for a particle entrapment is simply related to the impact length of the trajectory (L) compared to the bowl length(L_{bowl}).

As long as inter-particle interactions and particle fluid two-way coupling interactions are neglected, each particle trajectory can be computed independently. For a given particle size and density and a set of operating conditions (film thickness, flow rate and rotation rate of the bowl) each particle trajectory connects a certain position at the inlet of the film with an impact location on the wall. Therefore, it is straightforward to determine whether the particle is trapped or not (a particle is trapped in the bowl if the impact location occurs before the exit of the simulation domain corresponding to the length of the bowl wall). The probability of entrapment for each type of particle is then related to the probability of finding a particle located at a certain distance from the wall in the film at the bowl inlet. We chose a uniform particle distribution at the entrance (cf. §1.1) which means that the particulate flow rate is directly related to the fluid flow velocity profile (cf. figure 2).

1.4. Analysis of scaling laws

A number of assumptions have been required to set our simulation model but we can go even further in simplifying the problem to highlight the basic features which control the particle separation in the Falcon apparatus. Indeed, the most intrinsic trends controlling the entrapment of coarse and heavy particles at the wall can be obtained by the analysis of scaling laws. Those laws will relate the impact length to the basic operating conditions of the process and provide the sensibility of the results to each parameter. This is a theoretical estimate which can be compared to more accurate numerical modelling and experimental measurements. This section is dedicated to the determination of scaling arguments for the length (L) before impact at the wall. L is the result of a particle trajectory integration. Writing Y as the normal distance of the particle from the wall and X its streamwise position along the bowl wall direction, then L can be obtained by integrating the following equation:

$$\mathrm{d}X = \frac{v_X}{v_Y}\mathrm{d}Y \tag{7}$$

Assuming that the particulate Reynolds number based on the slip velocity between the particles and the fluid is small, we can use the Stokes sedimentation velocity obtained when the drag coefficient $C_D = 24/Re_p$. The two components of the particle velocity are given by the following equations:

$$v_X = u_X + \frac{F_X}{6\pi\mu r_p} \tag{8a}$$

$$v_Y = u_Y + \frac{F_Y}{6\pi\mu r_p} \tag{8b}$$

u_X is the streamwise velocity of the fluid which depends on the position of the section along the bowl wall but also on the distance normal to the wall. It may be expressed through equation (9a) (see Appendix for derivation details) as the product of the average velocity ($Q/\mathcal{A}_f$) and a wall normal profile (P) depending on the normalized position Y/h within the fluid film (constant thickness h).

$$u_X = \frac{Q}{2\pi r h\left(1 - \frac{h}{2r}\cos\frac{\beta}{2}\right)} P\left(\frac{Y}{h}, r\right) \tag{9a}$$

Considering a thin film ($h \ll r$), this yields:

$$u_X \approx \frac{Q}{2\pi r h} P\left(\frac{Y}{h}, r\right) \tag{9b}$$

In the streamwise direction of the flow, the slip velocity can be neglected because the slip is the result of a balance between the projection of the buoyancy effect, the centrifugal acceleration and the drag force. Due to the small value of the cone angle of the bowl, the particulate relative velocity is small compared to the average velocity of the carrying fluid flow. On the contrary, the

centrifugal force is dominating in the crossstream direction. Indeed, the assumption of a constant film thickness leads to very weak fluid velocities across the film. Consequently, we can make the following simplications in the trajectory equation modelling.

$$u_X \gg \frac{F_X}{6\pi\mu r_p} \tag{10a}$$

$$u_Y \ll \frac{F_Y}{6\pi\mu r_p} \tag{10b}$$

The projection of the centrifugal force experienced by the particles in the direction normal to the wall is:

$$F_Y = -\Delta\rho\, \mathcal{V}_p\, \omega^2 r \cos\frac{\beta}{2} \tag{11}$$

The impact length L results from a simple integral depending on Y_0, the initial particle distance away from the wall in the inlet section of the fluid film:

$$\mathrm{d}X = \frac{6\pi\mu r_p}{F_Y} u_X\, \mathrm{d}Y \tag{12a}$$

$$\int_0^L r^2\, \mathrm{d}X = \int_{Y_0}^0 \frac{9}{4\pi} \frac{-Q\,\mu}{\Delta\rho\, r_p^2\, \omega^2\, h\, \cos\frac{\beta}{2}} P\left(\frac{Y}{h}, r\right) \mathrm{d}Y \tag{12b}$$

The theoretical analysis could make one step forward by including the relation between the rotation rate of the Falcon bowl, the fluid flow rate and the thickness of the liquid film $h(\omega, Q)$. In the present study, we consider them as independent parameters. For the same reason of simplicity, we recall that the rotation of the flow in the azimuthal direction is approximated to a solid body rotation and the flow profile in the (X, Y) plane is a semi-parabola $P(Y/h, r)$ (Poiseuille flow between a wall and a free shear interface). We accounted for the effect of the cone angle on the average flow velocity as the film cross-section increases along the direction of the bowl wall.

$$r = R_0 + X \sin\frac{\beta}{2} \;\Rightarrow\; r^2 \approx R_0^2 + 2R_0 X \sin\frac{\beta}{2} \tag{13a}$$

$$P\left(\frac{Y}{h}, r\right) = \frac{3}{2}\left(2\frac{Y}{h} - \frac{Y^2}{h^2}\right) \tag{13b}$$

The result of the integration for a particle released at a distance Y_0 from the wall is:

$$L\left(1 + \frac{L}{R_0}\sin\frac{\beta}{2}\right) = \frac{27}{8\pi} Q\mu\Delta\rho^{-1} r_p^{-2} \omega^{-2} R_0^{-2} \left(\cos\frac{\beta}{2}\right)^{-1} \left(\frac{Y_0^2}{h^2} - \frac{Y_0^3}{3h^3}\right) \tag{14}$$

which in turn gives the following scaling laws:

$$L^{1+\alpha} \propto Q\,\mu\,\Delta\rho^{-1}\, r_p^{-2}\, \omega^{-2}\, R_0^{-2-\alpha} \tag{15a}$$

$$\text{where } \alpha = \frac{\ln\left(1 + \frac{L}{R_0}\sin\frac{\beta}{2}\right)}{\ln\frac{L}{R_0}} \tag{15b}$$

It is interesting to note in the expression (15a) that the sedimentation length of a particle is, according to this theory, independent of film thickness. Although the theory described here is a simplification of our simulation model and of the real physics of Falcon concentrators, this information can be used to strengthen our assumption of constant film thickness. Even if a relation exists between the evolution of the thickness and the Falcon's operating parameters, we can already draw some conclusions obtained with an approximated constant film thicknesses.

1.5. Application to ultrafine particle recovery

A simple analysis of the scaling law gives a first clue on the possibility of using a Falcon concentrator in the ranges of density and size we selected. Indeed, the expression (15a) shows a stronger dependence of the impact length on the particle width than on their relative density. The difference in exponents is rather small and a more thorough inspection of the simulation results based on the complete force balance is required for a definite answer. A separation based only on the nature of the particles for any size would be restricted to very large density differences.

2. Results and discussion

2.1. Numerical validation of the scaling laws

The full numerical simulations of the trajectory take into account all the relevant forces which depend both on the local flow characteristics and the particle dynamics. We have identified the dominant forces to be the enhanced gravity due to rotation, added mass and drag forces. In the theoretical prediction of scaling laws, the drag force has been approximated to the Stokes drag for low particulate Reynolds number. This expression is only accurate when $Re_p < 1$.

$$Re_p = 2\frac{v_Y\, r_p}{\nu} = \frac{4}{9}\left(\frac{\rho_p - \rho_f}{\rho_f}\right)\frac{\omega^2\, R_0\, r_p^3}{\nu^2} \tag{16}$$

Fixing $Re_p = 1$, equation (16) gives the relation between all the physical parameters involved in (14). Then, we can evaluate the the limit of the assumption

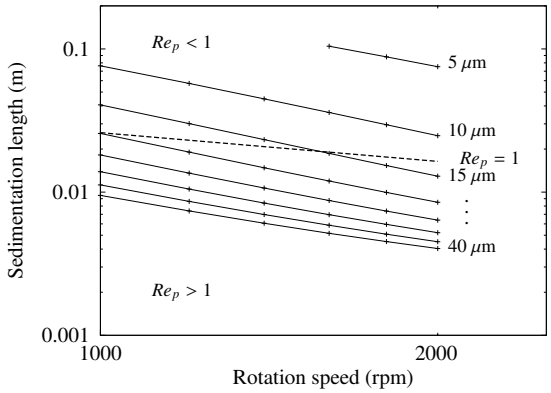

Figure 4: Variation of impact length (L) with rotation speed
Simplified simulation with $\rho_p = 1.3$ g/cm^3, $Q = 5$ l/min, $r_p = [5, 10, 15, 20, 25, 30, 35, 40]$ μm

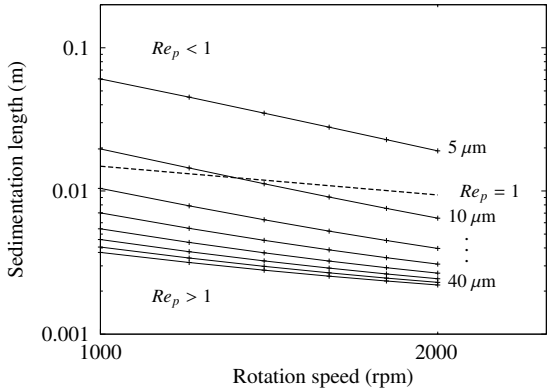

Figure 5: Same as figure 4, but $\rho_p = 2.6$ g/cm^3

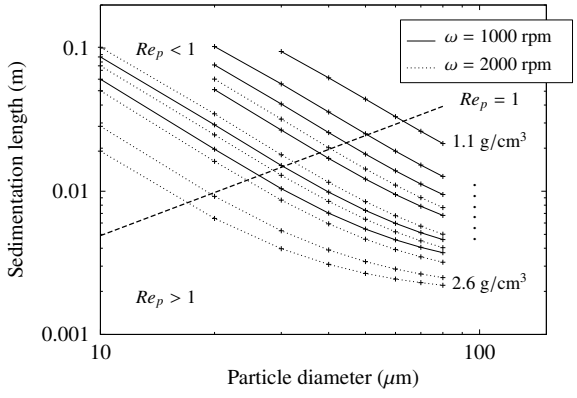

Figure 6: Variation of impact length (L) with particle diameter
Simplified simulation with $Q = 5$ l/min, $\rho_p = [1.1, 1.2, 1.3, 1.5, 2.0, 2.6]$ g/cm^3

$Re_p < 1$. This limit is materialized by a dash line in figures 4, 5 and 6.

Even small and light particles may settle onto the bowl wall at higher particulate Reynolds numbers while experiencing the Falcon's enhanced gravity field. Therefore, it is necessary to compare the predictions of the scaling laws with simulation results obtained using a more general expression of the drag force when eventually $Re_P > 1$.

For testing the accuracy of the scaling laws, we have carried out a number of simulations using the Poiseuille flow field we assumed in our theoretical analysis. In these cases, the differences between the simulation results and the theoretical predictions can be only inferred to the force balance expression. Figures 4, 5 and 6 show the simulation results. Clearly, these figures show that the rotation rate and the impact length are correlated with a constant exponent when the Stokes law is valid (as expected from §1.4). Particles of low particulate Reynolds number trapped into the bowl have a length before impact at the wall which is approximately the bowl length ($L_{\text{bowl}} = 7$ cm), so $\alpha = 0.25$. Their measured exponents in the simplified simulations are:

$$L^{1.25} \propto Q^{1.06}\, \Delta\rho^{-1.0}\, r_p^{-1.91}\, \omega^{-1.99} \tag{17}$$

When $Re_P > 1$ at some point of the trajectory, the drag force becomes non-linear and the simulations of the full force balance are necessary. The general trend is conserved although $Re_P > 1$ for light particles while the exponent varies more drastically for the heavier and larger particles for which the separation is more efficient. In the context of our study (particles in the range of 5 to 60 μm), we can conclude that the scaling laws are good estimates of the separation process.

Let E be the integral of the inlet velocity profile (P):

$$E(Y_0) = \frac{1}{h}\int_0^{Y_0} P\left(\frac{Y}{h}, R_0\right) \mathrm{d}Y \tag{18a}$$

When multiplied by the feed washability density distribution function, $E(Y_0)$ gives the mass fraction of particles whose inlet position is between 0 and Y_0. The inlet position Y_0 that corresponds to a given sedimentation length L can be calculated directly by inverting the scaling law $L(Y_0)$. In particular, $Y_0(L_{bowl})$ is the inlet elevation of those particles whose impact length is precisely equal to the bowl length. Hence, $E(Y_0(L_{bowl}))$ is the function which, when mutiplied by the feed washability probability density distribution function, yields the cumulative mass fraction of particles that hit the bowl. In minerals processing, this is better known as the partition

function (C) (Wills and Napier-Munn, 2006), which we define with the above notations as:

$$C = E\left(Y_0(L_{\text{bowl}})\right) \tag{18b}$$

When all the variables are independent of Y, which is true in our simplified simulation, equation (14) is of the generic type:

$$L(Y_0)^{1+\alpha} \propto Q^a\, \mu^b\, \Delta\rho^c\, r_p^d\, \omega^e\, R_0^f\, E(Y_0) \tag{18c}$$

The inverse function is of the type:

$$Y_0(L) \propto E^{-1}\left(Q^{-a}\mu^{-b}\Delta\rho^{-c}r_p^{-d}\omega^{-e}R_0^{-f}L^{1+\alpha}\right) \tag{18d}$$

where E^{-1} is the inverse of function E. By substituting (18d) into (18b), the partition function C can be deduced from the scaling law:

$$C \propto Q^{-a}\mu^{-b}\Delta\rho^{-c}r_p^{-d}\omega^{-e}R_0^{-f}L_{\text{bowl}}^{1+\alpha} \tag{18e}$$

Substituting the exponents of equation (14) into equation (18e) will not yield usable quantitative prediction of the partition function C, since equation (14) is based on a simplified model of the physics inside the Falcon bowl. In order to determine the true quantitative exponents that will allow us to use equation (18d) for predicting the Falcon's partition function in the ultrafine particle size range, a full simulation, coupled with a more complete theoretical analysis, is required.

2.2. Implications for ultrafines' gravity separation

Sedimentation length is strongly dependant on particle size in the domain of validity of the Stokes drag law (cf. §1.5). However figure 6 shows that it becomes less size dependant the further the particle flow conditions move away from the Stokes domain ($Re_p > 1$). By reducing the particle size dependency, it should then be possible to reveal an operating domain where the Falcon concentrator will perform as a gravity separator for ultrafine particles. Identification of this operating domain is the focus of our current work.

2.3. Discussion of the full simulation results

The full numerical model including the flow simulation can now be used to compute the impact length for any particle (size and a density). Depending on distance to the wall Y_0 at the inlet of the film and the Falcon's operating conditions, each particle will follow a specific trajectory through the liquid film until they impact the wall of the rotating bowl or eventually exit the bowl without being trapped. Their sedimentation length, compared to the actual bowl length (cf. figure 2) gives us a direct criterion for predicting whether the particle is trapped by the Falcon. With an input washability distribution in the feed stream, our simulation model allows us to predict the washability of both the product and the tailings streams. Consequently, the Falcon's partition function can be calculated. The symbols in figure 7 show the simulation results for the partition function of a L40 Falcon concentrator for particles whose densities correspond to a mixture of sandy and organic dredged sediments.

Scaling laws are also very useful from a simulation point of view. Indeed, the CPU time required for the simulation of a trajectory varies as the inverse of the square of the particle diameter (due to the constraint on the time step related to the particulate viscous relaxation time), the Lagrangian tracking of very fine particles is extremely time consuming. Based on scaling laws, the impact length for very fine particles, and hence their recovery, can be extrapolated from the simulations with coarser particles.

Experimental measurements will be valuable to test our model assumptions and the accuracy of the separation prediction. Comparison between simulation results and experimental measurements on a L40 Falcon concentrator is the object of ongoing work. Coming back to the purpose of our stydy, beneficiation of dredged sediments with a Falcon concentrator, our simulation results are encouraging as they predict a sharp separation around 10 μm in the particle density and size range of interest (see figure 7).

The partition function predicted by the simulations for 1000 rpm and 4 l/min was applied to the washability measured on a sample of dredged sediments from a lake. Figures 8 and 9 show the results we obtained. The concentrate contains all the valuable 100 μm $\times$ 10 μm sandy fraction while most of the organic content and ultrafine particles (smaller than 10 μm) are composing the tailing stream. These preliminary findings confirm that the Falcon concentrator is a promising process for the benaficiation of fine and ultrafine dredged sediments.

Conclusion and perspectives

In this paper, we have presented the bases of a mechanistic model for the Falcon separator, with the objective of quantifying its potential for beneficiating dredged sediments. The gravity separation challenge with dredged sediments comes mainly from the size of the material, with valuable sandy particles in the 100 μm $\times$ 10 μm size range. Particle fineness, along with the relatively high content of valuable material in

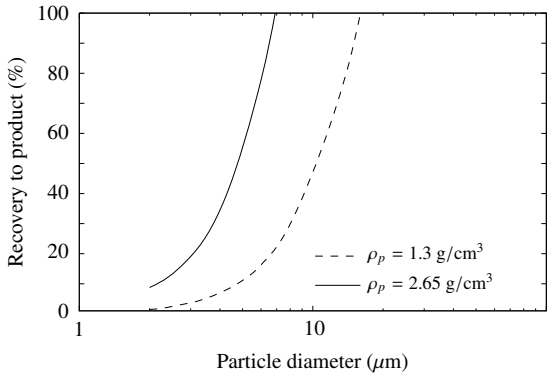

Figure 7: Examples of separation curves predicted by simulation
Full simulation result for ω = 1000 rpm and Q = 4 l/min, in a Falcon L40 concentrator with a smooth 7 cm long bowl.

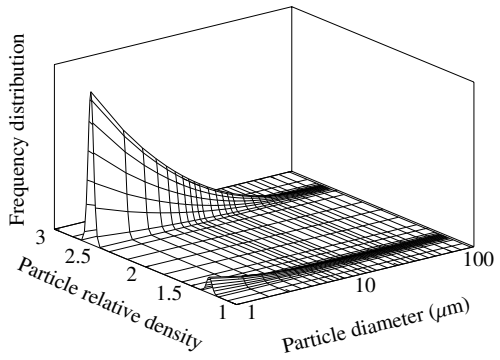

Figure 8: Washability of a sample of dredged sediments

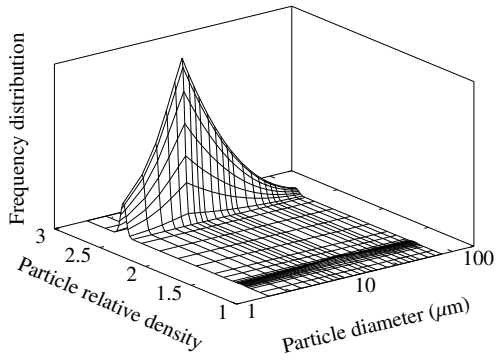

Figure 9: Predicted washability of the Falcon concentrate
Full simulation result using the same operating conditions as figure 7, applied to the feed washability given in figure 8.

the feed, make this problem quite different from standard Falcon applications.

Contrary to separation problems with larger and denser particles, dredged sediment particles have a comparatively low inertia; hence their separation inside the Falcon is mainly controlled by the fluid flow field. This explains why the mechanistic Falcon model that is presented here relies on a hydrodynamic analysis of particles' trajectories inside the Falcon's flowing film. The probability of recovering a particle with the Falcon is therefore directly related to the particle's probability of hitting the wall of the Falcon bowl.

Analysis of the fluid flow equations has revealed that accurate modelling of particle trajectory inside the Falcon is a truly three-dimensional problem, as the fluid velocity in the azimuthal direction appears in the axysimetric solution of the particle force balance equation. Nevertheless, the three-dimensionality of the problem was neglected in this paper in favour of providing the reader with a complete picture of the framework of the proposed phenomenological Falcon model. A forthcoming paper will present the full three-dimensional solution, whose results can be directly substituted in the model equations presented here. The paper presents a dimensional analysis of the particle impact length in somewhat simplified conditions, and the generic way by which the impact length scaling law can be used to derive the Falcon's partition function from fluid flow mechanics simulations.

Future work will involve extending the derivations proposed in the paper to the full three-dimensional case, for which early simulation results are already discussed in the last section of the paper. The results presented here are encouraging, as they indicate that the Falcon concentrator can indeed be used for beneficiating dredged sediments. Indeed, when the full three-dimensional flow field is used for calculating particle trajectories, we find that the Falcon concentrator is able to concentrate the valuable 100 μm $\times$ 10 μm sandy fraction while rejecting the organic particles (s.g. = 1.3) and ultrafine particles (¡ 10 μm). These conclusions are tentative only, and more simulations coupled with experimental validations will be carried out in order to validate a complete mechanistic separation model for ultrafine particle separation with the Falcon concentrator, from which the best operating conditions will be determined.

Acknowledgement

This work is funded by the French "Agence Nationale pour la Recherche" (ANR), in the framework of the PROPSED project.

Appendix

The fluid velocity profile is written as the product of the average velocity ($Q/\mathcal{A}_f$) and profile (P) depending on the wall normal distance Y scaled by the film thickness.

$$u_X = \frac{Q}{\mathcal{A}_f} P\left(\frac{Y}{h}, r\right)$$

The fluid film section ($\mathcal{A}_f$) is a truncated cone, whose generatrix is the film thickness normal to the bowl wall.

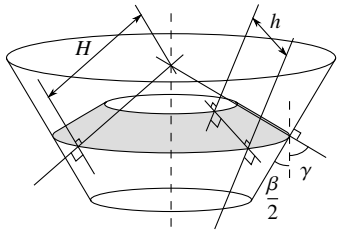

Defining $\mathcal{A}_l$ as the lateral area of a cone, we then find (see notations on figure above):

$$\begin{aligned}\mathcal{A}_f &= \mathcal{A}_l(H) - \mathcal{A}_l(H-h)\\ &= \frac{\pi r^2}{\sin\gamma} - \frac{\pi(r - h\sin\gamma)^2}{\sin\gamma} = \pi(2rh - h^2\sin\gamma)\\ &= 2\pi rh\left(1 - \frac{h}{2r}\cos\frac{\beta}{2}\right)\end{aligned}$$

which yields equation (9a).

Notations

The p and f subscripts stand respectively for physical properties of the particles and fluid. They may be omitted when there is no ambiguity (the viscosity for instance). The X and Y subscripts represent the vector components into the rotating frame : X for the streamwise direction and Y for the wall normal direction (see figure 3).

$\vec{u}, \vec{v}$: velocity vectors of the fluid and the particles
$\vec{u}_{2D}, \vec{v}_{2D}$: projections of the velocities onto the plane $(\vec{r}, \vec{z})$
u_θ, v_θ : azimuthal velocities, so that $\vec{u} = \vec{u}_{2D} + u_\theta \vec{e}_\theta$
p : pressure inside the fluid
ρ : density
μ : dynamic viscosity
ν : kinematic viscosity
r_p : particle radius
$\mathcal{V}, \mathcal{A}$: volume and area
C_M, C_D : added mass and drag coefficients
$\vec{F}_M, \vec{F}_D$: added mass and drag forces
$\vec{F}_B, \vec{F}_G$: buoyancy force and effect of the pressure gradient
C : recovery to product
E : feeding profile integral on the trapped particles
L : sedimentation length
α : sedimentation length exponent in scaling laws
L_{bowl} : bowl length
r : distance from the bowl symmetry axis
h : film thickness
P : velocity profile inside the film
X : position in the streamwise direction
Y : position in the film, wall normal distance
Q : feeding rate
ω : rotation rate
β : opening angle of the bowl
R_0 : bowl radius
Re_p : particulate Reynolds number

References

Abela, R. L., 1997. Centrifugal concentrators in gold recovery and coal processing. In: Extraction Metallurgy Africa.

Ancia, P. H., Frenay, J., Dandois, P. H., 1997. Comparison of the Knelson and Falcon centrifugal separators. In: Richard M. Mozley International Symposium.

Bradley, P., Patil, D. P., Ho, K., 2000. Development and demonstration of an enhanced gravity separator for coal cleaning. Tech. rep., Illinois Clean Coal Institute.

Bruin, S., 1969. Velocity distributions in a liquid film flowing over a rotating conical surface. Chemical Engineering Science 24, 1647–1654.

Chatterjee, A., 1998. Role of particle size in mineral processing at Tata Steel. International Journal of Mineral Processing 53, 1–14.

Clift, R., Grace, J. R., Weber, M. E., 1978. Bubbles, Drops and Particles. Academic Press.

Coulter, T., Subasinghe, G. K. N., 2005. A mechanistic approach to modelling Knelson concentrators. Minerals Engineering 18, 9–17.

Deveau, C., 2006. Improving fine particle gravity recovery through equipment behavior modification. In: 38th Annual Meeting of the Canadian Mineral Processors. Paper 31. pp. 501–517.

Dijk, P. E., Janse, A. M. C., Kuipers, J. A. M., van Swaaij, W. P. M., 2001. Hydrodynamics of liquid flow in a rotating cone. International Journal of Numerical Methods for Heat & Fluid Flow 11 (5), 386–412.

Holtham, P., Gee, B., Dunne, R., Gregory, S., 2005. Recovery of fine gold particles using a Falcon 'B' separator. In: Deschenes, G. (Ed.), International Symposium for the Treatment of Gold Ores.

Honaker, R. Q., Das, A., 2004. Ultrafine coal cleaning using a centrifugal fluidized-bed separator. Coal Preparation 24 (1–2), 1–18.

Honaker, R. Q., Patil, D. P., 2002. Parametric evaluation of a dense-medium process using an enhanced gravity separator. Coal Preparation 22 (1), 1–17.

Honaker, R. Q., Paul, B. C., Wang, D., Huang, M., 1994. Application of centrifugal washing for fine coal cleaning. In: Society for Mining, Metallurgy and Exploration Annual Meeting.

Honaker, R. Q., Reed, S., 1995. A fine coal circuitry study using column flotation and gravity separation. Tech. rep., Department of Energy.

Honaker, R. Q., Wang, D., 1998. Falcon concentrators: a high capacity fine coal cleaning technology. In: Society for Mining, Metallurgy and Exploration Annual Meeting.

Honaker, R. Q., Wang, D., Ho, K., 1996. Application of the Falcon concentrator for fine coal cleaning. Minerals Engineering 9 (11), 1143–1156.

Janse, A. M. C., Biesheuvel, P. M., Prins, W., van Swaaij, W. P. M., 2000. Granular flow in a rotating cone partly submerged in a fluidized bed. American Institute of Chemical Engineers Journal 46 (3), 499–508.

Langrish, T. A. G., Makarytchev, S. V., Fletcher, D. F., Prince, R. G. H., 2003. Progress in understanding the physical processes inside spinning cone columns. Chemical Engineering Research & Design 81 (1), 122–130.

Laplante, A. R., Buonvino, M., Veltmeyer, A., Robitaille, J., Naud, G., 1994. A study of the Falcon concentrator. Canadian Metallurgical Quarterly 33 (4), 279–288.

Laplante, A. R., Nickoletopoulos, N., 1997. Validation of a Falcon model with a synthetic ore. Canadian Metallurgical Quarterly 36 (1), 7–13.

Laplante, A. R., Shu, Y., 1993. A comparative study of two centrifugal concentrators. In: 25th Annual Meeting of the Canadian Minerals Processors. Paper 5. pp. 18–36.

Luttrell, G. H., Honaker, R. Q., Phillips, D. I., 1995. Enhanced gravity separators: New alternatives for fine coal cleaning. In: 12th International Coal Preparation Conference. pp. 281–292.

Magnaudet, J., Rivero, M., Fabre, J., 1995. Accelerated flows past a rigid sphere or a spherical bubble. part 1. steady straining flow. Journal of Fluid Mechanics 284, 97–135.

Majumder, A. K., Lyman, G. J., Brennan, M., Holtham, P. N., 2006. Modeling of flowing film concentrators part 1. water split behavior. International Journal of Mineral Processing 80 (1), 71–77.

Makarytchev, S. V., Langrish, T. A. G., Prince, R. G. H., 1998. Structure and regimes of liquid film flow in spinning cone columns. Chemical Engineering Science 53 (8), 1541–1550.

Makarytchev, S. V., Xue, E., Langrish, T. A. G., Prince, R. G. H., 1997. On modelling fluid flow over a rotating conical surface. Chemical Engineering Science 52, 1055–1057.

McAlister, S. A., Armstrong, K. C., 1998. Development of the Falcon concentrator. In: Society for Mining, Metallurgy and Exploration Annual Meeting.

Venkatraman, P., Kow, W. S., Sadowski, J., Anthraper, A., 2000. Application of Floatex/spiral circuit in processing silica sand. In: Society for Mining, Metallurgy and Exploration Annual Meeting.

Wills, B. A., Napier-Munn, T. J., 2006. Wills' mineral processing technology : an introduction to the practical aspects of ore treatment and mineral recovery, 7th Edition. Butterworth-Heinemann, Oxford.

Zhao, Y.-M., Wen, X.-F., Shi, H.-X., Jiao, H.-G., Tao, Y.-J., 2006. Study on metals recovery from -0.074 *mm* printed circuit boards by enhanced gravity separation. The Chinese Journal of Process Engineering 6 (2), 201–204.